JJMIE

Volume 18, Number 2, June. 2024
ISSN 1995-6665
Pages 251- 266
https://doi.org/10.59038/jjmie/180201
Editor-in-Chief: Prof. Ali M. Jawarneh

Jordan Journal of Mechanical and Industrial Engineering

Radial basis Neural Network Model to Prediction of Thermal Resistance and Heat Transfer Coefficient of Oscillating Heat Pipe Using Graphene and Acetone-Based Nanofluids

Parashuram A Kutakanakeri[*1], K. Rama Narasimha[2], K. Gopalakrishna[3], Laxminarayana K.G Bhatta[4]

[*1]*Department of Mechanical Engineering, K S School of Engineering and Management, Bangalore -560109 Visvesaraya Technological University, Belagavi-590018, Karnataka, India*
[2]*Department of Mechanical Engineering, K S School of Engineering and Management, Bangalore -560109, Visvesaraya Technological University, Belagavi-590018, Karnataka, India*
[3]*Department of Mechanical Engineering, Jyothy Institute of Technology, Tataguni, Off Kanakapura Road, Bangalore - 560082, Visvesaraya Technological University, Belagavi-590018, Karnataka, India*
[4]*Center for Incubation, innovation, Research and consultancy, Jyothy institute of technology Bengaluru-560082, Visvesaraya Technological University, Belagavi-590018, Karnataka, India*

Received 15 Jan 2024 *Accepted 1 Mar 2024*

Abstract

The primary objective of this study was to assess the operational efficiency of an oscillating heat pipe featuring an inner diameter of 1.7 mm and an outer diameter of 3 mm. This OHP was filled with an acetone-based fluid infused with graphene nanoparticles. The research aimed to analyze the effects of altering filler ratio and heat inputs on temperature difference, heat transfer coefficient, and thermal resistance in an oscillating heat pipe, with a specific focus on filler ratios ranging from 50% to 80% and heat inputs between 20W and 40W. The results reveal that there is a maximum in heat transfer coefficient of 220.48W/m^2^{o}C and 224.1 W/m^2^{o}C for acetone and graphene respectively. There is a decrease in thermal resistance 0f 1.441^{o}C/W and 1.421^{o}C/W for acetone and graphene for optimal combinations (40W with 80% filler ratio). Finally, the experimental data of 1800 datasets were used to develop the Artificial Neural network model using Radial basis function by considering three input parameters viz, fill ratio (50% to 80%), heat load (25W to 40W) and time with an output of temperature difference, heat transfer coefficient and thermal resistance. The developed ANN using the radial basisfunction (RBF) was able to predict the experimental parameters of temperature difference, heat transfer coefficient andthermal resistance with 97.70% and 97.12% accuracy for graphene and acetone respectively. Based on the obtainedresults MSE values for graphene and acetone are 1.015 and 1.064 respectively.

Keywords: Nano fluids, oscillating heat pipe, Thermal resistance, Heat transfer coefficient.

1. Introduction

In the realm of electronic product development, effective thermal management stands as a significant contemporary challenge. The production of excess heat by electronic devices and circuits has significantly increased. From microprocessors to advanced power converters, all electronic devices generate heat, and efficiently managing this heat is essential for their effective and dependable functioning. As electronic designs continue to enable improved performance within smaller form factors, efficient heat dissipation has become a fundamental consideration in the design process. A multitude of modern electronic devices now necessitate cooling that surpasses the capacities of conventional metal heatsinks. Among the solutions to disperse excessive heat, employing heat pipes has emerged as an effective strategy, where these pipes directly connect to the heat source for heat dissipation. Another promising avenue in the realm of heat transfer devices, particularly for applications like electronics cabinet cooling, is the employment of oscillating or pulsating heat pipes (PHPs). Despite their unassuming appearance, these devices display fascinating thermos-hydrodynamic operational traits. A PHP contains an incomplete fill of a working fluid, which autonomously organizes into alternating liquid and vapor slugs within its capillary tubes. In this configuration, the evaporator section, located at one end, absorbs heat and transfers it to the opposite end, the condenser section, through the rhythmic motion of the liquid-vapor system. Fundamentally, a Pulsating Heat Pipe (PHP) operates as a device that transfers heat out of balance, functioning through a sophisticated combination of different two-phase flow instabilities. Its effectiveness

* Corresponding author e-mail: Parashuram.a.k@gmail.com.

hinges on the consistent preservation of these non-equilibrium states. Pressure pulsations within the system facilitate the movement of liquid and vapor slugs. The device's design essentially guarantees that no external mechanical energy source is necessary for liquid transport; instead, the driving pressure pulsations are solely thermally induced. Both single and multiple-loop PHP investigations have been extensively documented in the literature, shedding light on how various design parameters can influence its performance.

Performance of experimental initiation heat pipes utilizing a distinct molten salt mixture as the working medium was examined. The trials encompassed varying charge quantities from 40g to 80g. Among the combinations explored, the 40g configuration demonstrated a favorable outcome. The design formulated for this investigation showcased enhanced heat transfer characteristics through the utilization of a 40g working fluid mixture [1]. Experimenting with diverse working liquids including ethanol, methanol, acetone, and deionized water, a closed-circuit pulsating heat pipe with a diameter of 2mm and fill levels ranging from 20% to 95% was assessed. The heat input ranged from 5W to 100W. The heat input's rise engendered an impact on dynamic viscosity, in addition to the energy carried by the working medium, involving specific heat and latent heat of vaporization. Notably, at lower filler loadings, a lower boiling point was observed alongside decreased latent heat of vaporization, leading to eventual dry-out in the exit state [2].

Future demands necessitate advanced cooling techniques for micro heat channels in electronic devices, focusing on enhanced thermal properties and the generation of high heat flux for improved heat transfer capabilities specific to applications [3].

A novel design has been devised to optimize the utilization of a microplate loop heat pipe for efficient heat pipe applications involving sintering temperature and insulated wick in electronic chip cooling [4]. Conducting a numerical analysis, heat transfer prediction in pulsating heat pipes was undertaken. A governing equation was formulated encompassing mass, momentum, and energy considerations for both water and ethanol, accounting for liquid and vapor slugs. Ultimately, the fluids based on water and vapor exhibited heat transfer rates of 98% and 94%, respectively [5]. To enhance the thermal performance of the newly developed closed-loop thermosyphon, an innovative approach was adopted. Two distinct methods were employed: in the first, the heating elements were symmetrically bent at each curve, while in the second, the heating elements were asymmetrically placed along the U-tube due to gravitational orientation. Notably, the non-symmetrical arrangement of the heating elements led to superior and more efficient liquid circulation during the process, as observed. However, in the vertical position, there was a heat flux dissipation attributed to pool boiling, which was constrained to 75%, thereby maintaining the tube wall temperature below 80°C [6]. A comprehensive mathematical model in fluid dynamics was developed to examine how transient thermal and flow characteristics affect the thermal stability of an enclosed catalyst. The outcomes underscore that the heat generated at individual points is significantly influenced by the transient flow properties in the interconnected closed loop state. [7]. For both two-dimensional and three-dimensional temperature distributions, as well as pressure and velocity, the convection heat pipe's characteristics were established. The formulated model has the capability to anticipate thermal resistance across various heat source thresholds in heat pipes. Furthermore, this technique can serve in deducing capillary parameters for the specified structure through wall temperature measurements [8]. A novel testing setup was created to assess the thermal performance of partially open tubes by measuring temperature, pressure, and mass flow. The MATLAB-based simulation algorithm was detailed, and the effectiveness of the developed testing apparatus was evaluated by comparing the proposed method to acoustic phenomena [9]. For the assessment of PHP's predictive capabilities, a heat transfer model for a 1D mass-spring damper system was formulated. Four distinct models were established: those accounting for oscillatory motion, translational motion, combinations of both, and no motion. The findings suggest that with translational motion and a combined approach, the peak PHP is achieved as the extent of movement increases under the conditions of both modes being satisfied [10]. To ascertain the upper limit of heat transfer within the heat pipe, a mathematical model was constructed for a mesh wick configuration. The outcomes revealed that the heat transfer capacity was affected by variables including evaporator temperature, tilt angle, mesh layer, mesh size, and mesh count [11]. To enhance the efficiency of the heat pipe, it was imperative to determine the thermophysical properties required for evaluating the working fluid's performance. To accomplish this objective, a proficient dimensional analysis approach was employed, culminating in the creation of a validated one-dimensional mathematical model for the trapezoidal microgroove heat pipe. This model, distinguished by its elevated thermal conductivity, reduced surface tension, low latent heat of vaporization, heightened viscosity, and lower liquid density, introduced a highly advantageous and improved design, ensuring exceptional performance in the specific heat pipe application [12]. In a situation involving an oscillating heat pipe with varying liquid input (75% volume) in a 4-pass copper system, the power was increased from 60 W to 300 W, and frequencies were varied from 1.5 Hz to 2.5 Hz. The findings indicated that the temperature recorded by the thermocouple positioned outside the tube was 4-12% lower when compared to the measurements taken inside. The effective thermal conductivity calculated for the outside measurement was 14,000 W/m K, and for the inside measurement was 15,300 W/m K [13]. The heat transfer efficiency of a satellite heat pipe can be enhanced through the careful consideration of several parameters, including wick thickness, diameter, the quantity of wicks, wall thickness, length of the condenser and evaporator, and the core diameter of the steam section. Finally, a comparison between two was carried out. To evaluate the performance, a working medium consisting of ammonia and methanol was tested and the optimum value was determined. The results unequivocally demonstrate that when considering the total mass of the heat pipe, a decrease in thermal resistance of roughly 82.17% to 57.16% was noted for ammonia in comparison to methanol combinations [14]. In the context of a transparent 5-turn polydimethylsiloxane (PDMS) optical heat pipe (OHP), we investigated a fabricated system with dimensions of 190

mm x 155 mm, featuring a 2 mm diameter channel. In this study, we introduced Al_2O, ethanol, and a combination of both as working fluids, with a filler content of 70% being considered. Our findings indicate that the generation of an electric field and the choice of working medium do not impact the heat transfer efficiency throughout the process. [15]. Pulsating heat pipe tests were conducted using different concentrations and filling ratios of ethanol, methanol, cetyltrimethylammonium chloride (CTAC), and C19H42CIN, comparing them to ionized water. Thermal properties were examined for a closed-circuit heat pipe with 35%, 50%, and 65% filling fractions. The lowest thermal resistance occurred at 50% filling fraction, achieving 0.34 K/W under high heat loads. [16]. By introducing various inclinations (0°, 30°, and 45°) in the condenser section, methanol at 50% filling level was employed as the working fluid in a closed-loop pulsating heat pipe. The findings emphasized the pivotal role of gravity and fluid thermophysical properties in distinct heat loads and inclinations, contributing to performance evaluation. Notably, a 45° incline demonstrated improved heat transfer effectiveness in the closed-loop pulsating heat pipe [17]. An innovative approach was employed, involving additive manufacturing of multi-layer Ti-6AI-4V tubes for oscillation, accommodating different working fluids including acetone, water, and n-pentane. This layer-by-layer technique introduced a secondary wicking structure that acted as a capillary, facilitating fluid pumping within the OHP system [18]. To induce further imbalanced differential pressure, encompassing forces like capillary and gravitational pressure, implementing a PHP would involve the straightforward installation of an opposing heat source assembly within a convection tube design. This system would operate with a thermal conductivity of 12,603 W/mºK and a thermal resistance of 0.0729 W/K [19]. Considering these perspectives, conducting experimental visualizations seems highly appropriate. It enables the measurement and analysis of flow properties with substantial evidence, ultimately leading to improved performance in the developed systems. [20]. Apart from all these performance methods of Close loop pulsating heat pipe (CLPHP) can also be evaluated using Al_2O_3 and deionized as a nanofluid to measure the performance of working fluids. Based on the observations thermal resistance was measured around 48% less than that of water [27]. In some cases, numerical methods have been introduced to predate the oscillatory movement of the fluids. Based on the observations, the study suggests that in fluids with high anti-thixotropic properties, harmonics are significantly altered, potentially leading to chaotic behavior in the bubble. For instance, under conditions of $Rx = 0.001$ and $\xi = 1/81$, a one-micron-sized bubble could expand to nearly 30 times its initial size [28]. The current research centers on analyzing the unconfined laminar flow of nanofluid and the heat transfer attributes surrounding a square cylinder, exploring the effects of different angles of incidence within the unsteady regime [29]. The heat transfer rate from the cylinder is augmented either with an increase in Richardson number or Reynolds number [30]. The influence of thermal radiation, velocity slip, Weissenberg number, power-law index parameter, and magnetic field on the boundary layer flow and heat transfer of tangent hyperbolic fluid with zero normal flux of nanoparticles past a stretching sheet were the parameters may influence the flow of nano fluids [31]. Pulsation frequency and amplitude, Reynolds number, Darcy number, medium porosity, nanoparticles fraction, and geometric ratio affect the system's thermal performance. It discovers direct correlations between heat transfer rate and pulsation amplitude, medium porosity, Darcy number, nanoparticles fraction, and geometric ratio, while the pulsation frequency has a neutral effect [32]. Numerical results and graphical representations are obtained for velocity, temperature, and concentration distributions, as well as skin friction, local Nusselt number, and local Sherwood number, across various values of governing parameters. The findings indicate that velocity decreases with an increase in first and second-order velocity slip and suction, while it increases with an increase in the power-law parameter [33]. Three-dimensional computations were conducted on a single flow passage with periodic boundary conditions to predict the thermal resistance and pressure drop of the heat sinks. The results indicate that increasing the flow velocity simultaneously decreases the thermal resistance and increases the pressure drop [34]. Apart from all this work some of the suitable materials also can be used for the heat transfer and storage medium in a moving bead heat exchanger for the solar power plants [35]. When it comes to numerical analysis is concern temperature rises with increasing radiation parameter (R), magnetic parameter (M), thermophoresis parameter (Nt), Brownian motion parameter (Nb), and Eckert number (Ec) [36].

Based on the previous investigations the comparative study of acetone and graphene was not discussed in terms of filler ratio, heat input [37, 38]. Hence, the present work discussed the multi-turn copper PHP is considered for experimental investigations. Acetone and Graphene-based nanofluids are selected as working fluids for Pulsating Heat Pipe (PHP) operations. Experiments under transient conditions are conducted for various heat inputs. Both the thermal resistance and heat transfer coefficient are assessed, with the findings being corroborated through an Artificial Neural Network (ANN) model on a radial basis. This Radial basis function-ANN has the ability to simultaneously estimate both thermal resistance and heat transfer coefficient, with a particular focus on analyzing the temperature deviation between evaporator and condenser. This investigation aims to identify superior parameter settings for nanofluids using Graphene and Acetone as base fluids. The parameters examined include filler content, heat load and time duration. This research provides a valuable opportunity to predict the most effective parameters, thereby reducing the time required for laboratory experiments. This initiative represents the integration of practical experiments and computational modeling and includes every conceivable combination of parameters.

2. Materials and method

In the present investigations, two types of liquids such as acetone and graphene particle based nano fluid were used to determine the heat transfer coefficient, temperature difference and thermal resistance for different filler ratios and thermal stress conditions. The purity of the graphene is 99% with a diameter of ~15 nm, while the purity of the acetone was around 99% and was considered in this study.

The detailed technical specifications of the condenser, the evaporator and all the equipment details with liquid properties are shown in Table 1. The selection criteria for the detailed experiments on the heat transfer performance of Oscillating Heat Pipes (OHP) using acetone and graphene as working fluids focused on two key variables: filler ratio and heat load conditions. Filler ratio represents the percentage of the OHP's internal volume that is occupied by the working fluid. By experimenting with a range of fractions, from a relatively balanced 50% to a more fluid-dominated 80%, the study aims to observe how the heat transfer efficiency varies with different levels of fluid saturation. The heat load conditions are critical for evaluating the OHP's performance under different thermal stresses. The range from 25 to 40 Watts, increasing in steps of 5 Watts, provides a gradient of thermal inputs to assess how the OHP copes with escalating heat levels. the selection of these specific filler fractions and heat load conditions enables a comprehensive evaluation of the OHP's efficiency and effectiveness in transferring heat.

In the present investigations, acetone-based fluid has been considered because of its high volatility makes it well-suited for use in heat pipes. When acetone is exposed to heat in the hot end of the heat pipe, it evaporates quickly, forming vapor that travels to the cold end. This rapid vaporization enhances the heat transfer coefficient, allowing for efficient heat removal from the hot end. The high volatility of acetone ensures rapid phase change, facilitating efficient heat transfer within the heat pipe. Additionally, acetone's low boiling point allows for operation at relatively low temperatures, making it suitable for cooling applications where precise temperature control is necessary.

3. Experimental Procedure.

Preparation of a nanofluid with graphene involves dispersing them into acetone with Sodium Dodecyl Sulfate (SDS) as a surfactant. Techniques like magnetic stirring, probe sonication, and ultra-centrifuging ensure nanoparticle dispersion and stability. graphene are chosen for their unique properties: high aspect ratio, strength, and conductivity. Acetone is chosen for its availability, safety, and compatibility. SDS lowers surface tension between acetone and graphene, aiding dispersion. Add optimized SDS amount to water to prevent excessive foam. Introduce graphene based on desired concentration. Place container on a magnetic stirrer with a magnetic stir bar for mixing and the final prepared nanofluid with steps is shown in Fig.1.

The set-up described in the specifications makes it possible to carry out heat transfer experiments with different liquids. Based on previous research, acetone and graphene-based Nano fluids exhibit enhanced thermal conductivity due to their unique properties. These two Nano fluids were selected in the present investigations. Fig. 3 presents a detailed schematic of the experimental setup. In this setup, copper is utilized for the capillary tubes in both the evaporator and condenser sections, with these tubes having an inner diameter of 2 mm and an outer diameter of 3 mm, as shown in Fig. 2. The total length of the closed-loop pulsating heat pipe is 2060 mm, with each of the evaporator and condenser sections being 500 mm long. A glass tube, which is 1000 mm long, is used to enable observation of the flow inside the Oscillating Heat Pipe (OHP) and is placed connecting the evaporator and condenser sections. This glass tube is made of borosilicate glass with an inner diameter of 2 mm and an outer diameter of 3 mm. The connection between the glass and copper tubes is made using silicon rubber tubes with an inner diameter of 2 mm and an outer diameter of 4 mm. Additionally, they exhibit leak-proof characteristics and can withstand elevated temperatures. Controlled heating is accomplished through a mica heater with a power rating of 350 W, designed for heating the working fluid. Temperature measurements are facilitated by four K-type thermocouples, capable of operating within a temperature range of -50 to 500°C with a maximum error of 0.10°C. Within the experimental setup, four thermocouples are securely positioned in the evaporator section, while two are placed in the condenser section. The temperatures recorded by two specific thermocouples in the evaporator section are denoted as T1 and T2, respectively. The temperatures recorded by two thermocouples in the condenser section are denoted as T3 and T4, respectively. These thermocouples are affixed to the walls of the copper tube. To ensure consistency, experiments are repeated, and temperature readings at various locations are obtained through the thermocouples. A data logger, specifically an Omega data logger (OM-SQ2020) with an accuracy margin of 0.10°C, is employed to log the test data. Throughout the entire setup, glass wool is uniformly applied to ensure effective insulation of the experimental arrangement.

Table 1. Detail technical specification of condenser and evaporator section

Condenser Section			**Evaporator section**	
Inner diameter		2mm	Material	Copper tube
Outer diameter		3mm	Inner diameter	2mm
Length		500mm	Outer diameter	3mm
Inner dia. copper tube		2mm	Length	500mm
Outer dia. copper tube		3mm		
Borosilicate glass dia.		2mm		
Borosilicate glass length		1000mm		
Heater			**Insulator**	
Type		Mica Heater	Teflon	100*50cm
Capacity		1000 W	Glass Wool	K=0.042W/mK
Data Acquisition system			**Thermocouples**	
Multi-channel data logger		24 bit	Type	K Type
Output		8 O/P	Range	-50ºC to 950ºC
Fluidused	Boiling Point (°C)	Melting Point (°C)	Temp. Range (°C)	Specific HeatCp (J/Kg K)
Acetone	54	-92	0-126	2030
Graphene	4200	3652	0-2600	2100

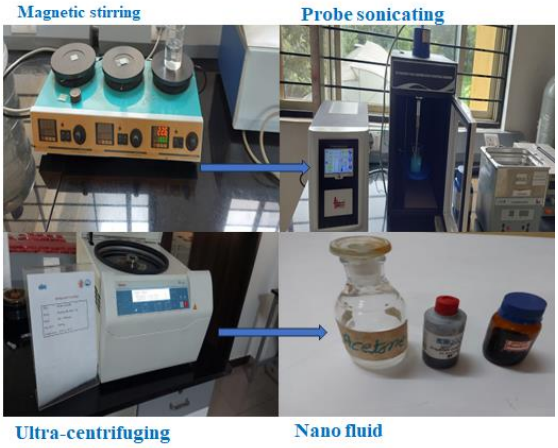

Figure 1. Nano fluid Preparation

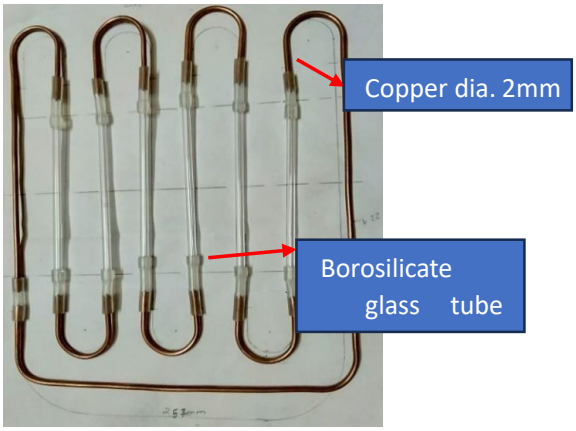

Figure 2. Copper tube with borosilicate glass tube

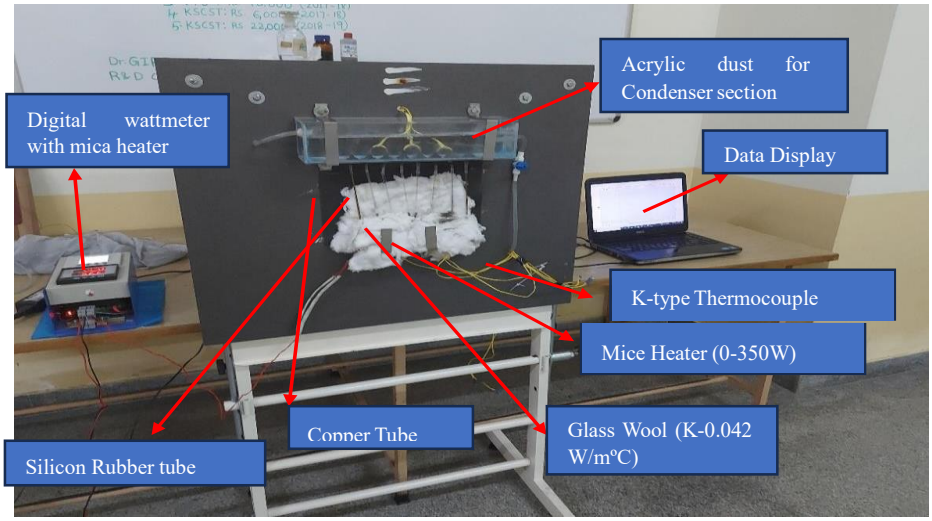

Figure 3. Experimentation setup with all necessary arrangement

4. Results and analysis

The detailed experiments were conducted based on different filler fractions of 50%, 60%, 70% and 80% and heat load conditions of 25 to 40 W with an interval of 5 W to determine the heat transfer performance of OHP for acetone and graphene. The experiment was conducted over a 30-minute duration, during which temperature data was continuously recorded by the data logger at one-second intervals. To examine the temperature disparity between the evaporator and condenser sections, alterations in load and fill ratio conditions were implemented. The extensive analysis involved the computation of three crucial output parameters: the temperature difference between the evaporator and condenser sections, the heat transfer coefficient, and the thermal resistance. These parameters were evaluated for both graphene and acetone nanofluids. Finally, the experimental result was validated using an artificial neural network (radial basis function). This approach was chosen to improve understanding of the validation process. In order to provide a deeper insight into the experimental investigations, a detailed breakdown of the experimental procedures for each individual parameter is presented below.

4.1. Temperature difference for different Filler ratio of acetone and graphene-based nanofluid

Transient experiments involved varying working fluids, namely Acetone and Graphene-based nanofluids, and recording temperature fluctuations over time. The experiments persisted until a steady state was attained. In Fig. 4, the time-dependent temperature difference between the evaporator and condenser is depicted for graphene and acetone under different heat inputs. Observations were conducted while adjusting the heat input from 25 W to 40 W for filler proportions ranging from 50% to 80%.

When operating with a filler ratio of 70% and heat input of 35 W and 40 W, the maximum temperature fluctuation was observed after 200 seconds, as shown in Fig. 4. The steady-state temperature of acetone for filler proportions of 50% and 60%, 70% and 80% were 98.27°C, 81.43°C, 77.36°C and 57.64°C, respectively. Similarly, the steady-state temperatures for graphene were 76.83°C, 67.18°C, 66.68°C, and 56.84°C. The steady-state temperature fluctuations for different filler ratios and heat input of acetone and graphene with increasing heat input are shown in Fig. 4. Upon examining all possible fluid combinations, it became evident that with an escalation in the heat load, there was a proportional rise in the temperature difference between the evaporator and condenser sections.

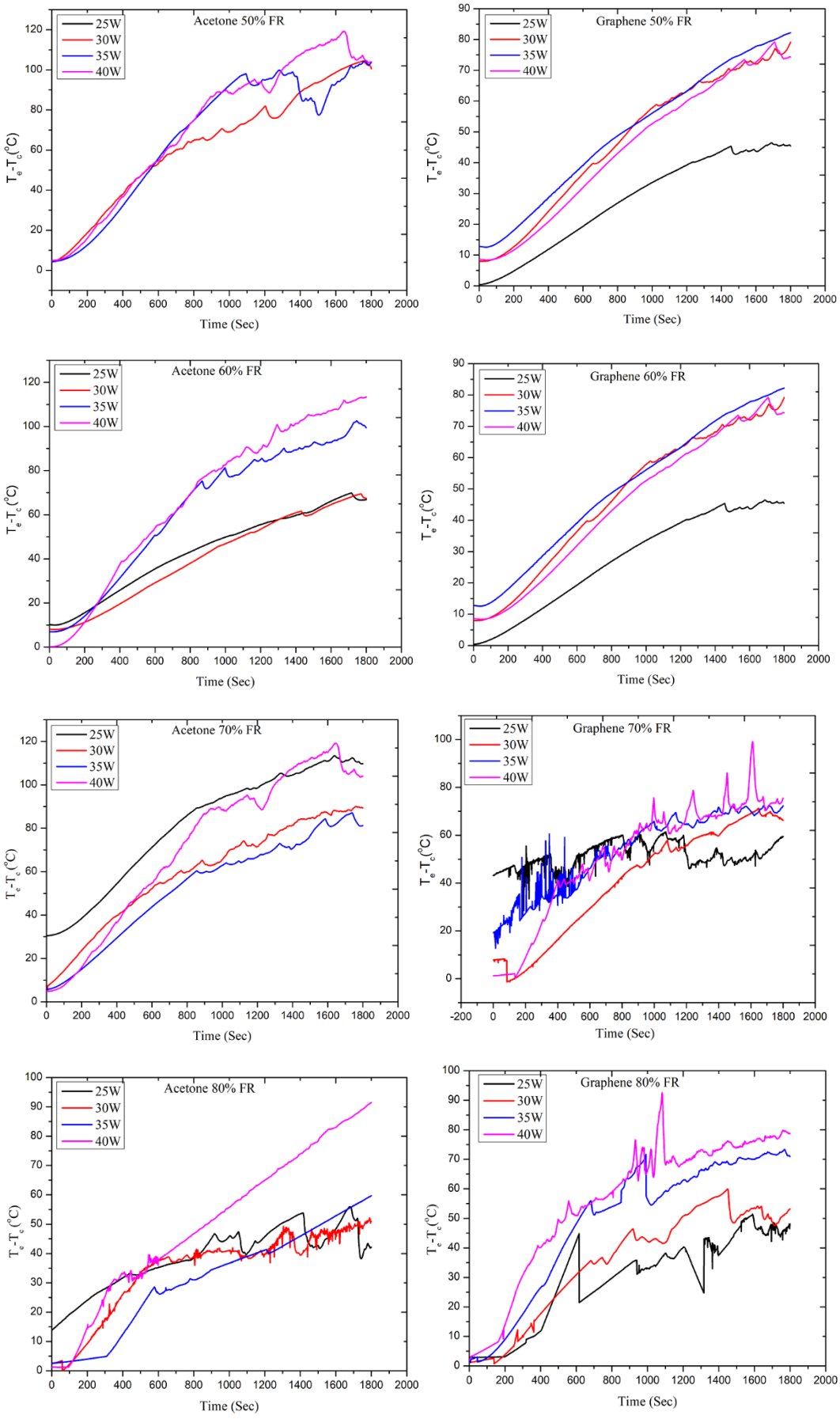

Figure 4. Difference in temperature for acetone and graphene based nano fluid at different filler ratio and heat loadconditions

4.2. Influence of fill ratio on thermal resistance of acetone and graphene based nano fluid

The thermal behavior of a Pulsating Heat Pipe (PHP) can be evaluated by analyzing its thermal resistance and heat transfer coefficient. The determination of a PHP's thermal resistance involves

$$R=\frac{TE-TC}{Q}\ ^{\circ}C/W \quad (1)$$

Fig. 5 shows a graphical representation of thermal resistance [24, 25, 26] and heat input corresponding to different filler ratios of PHP for acetone and graphene. The figure shows that the overall thermal resistance of the heat pipe decreases as the concentration of the nano-fluid increases along with the heat load. As the heat load increases, the nanoparticles enable better mixing of the fluid and contribute to improved heat dissipation, thereby reducing thermal resistance. The experimental results show that the lowest overall thermal resistance was achieved at 1.9392 and 1.666 0C/W for acetone and graphene filler content of 70% and further decreased to 1.4412 0C/W for a filler content of 80%. To ensure the accuracy and reliability of the newly introduced equipment and methods, the experiments were carried out three times. It is noteworthy that for graphene with a filler content of 80% and 40 W, a significant reduction in thermal resistance of 1.4210 C/W compared to acetone with a filler content of 80% and 40 W, a significant reduction in thermal resistance of 1.44120 C /W is recorded. W can be seen (Equation 1). This inherently high thermal conductivity allows graphene-based nanofluids to transfer heat more effectively than acetone, a common organic solvent with lower thermal conductivity. Although the filler content of graphene is slightly lower (70%) compared to acetone (80%), the specific properties of graphene nanoparticles in this concentration range can lead to better heat transfer performance. Graphene nanoparticles could enable multiple heat transfer mechanisms such as phonon transport and enhanced convection, contributing to a more significant reduction in thermal resistance compared to acetone. Consequently, a decrease in thermal resistance can be observed with increasing filler content, which is particularly noticeable at higher filler contents and a heat input of 40 W, as shown in Fig. 5.

4.3. Influence of fill ratio on heat transfer coefficient for acetone and graphene based nano fluid

The convective heat transfer coefficient of PHP is given by

$$h=\frac{Q}{A(TE-TC)}\ W/m^2C \quad (2)$$

In Fig. 6, the heat transfer coefficient variation at steady state is depicted for Acetone and Graphene across various heat loads, spanning a fill ratio range of 50% to 70%. The information indicates a significantly greater heat transfer coefficient for Graphene in contrast to Acetone. This divergence is attributed to the reduced temperature differential between the evaporator and condenser in the Graphene scenario, resulting in an increased heat transfer coefficient. Notably, as the heat input increases, there is a corresponding elevation in the heat transfer coefficient (Eq. 2), reaching 220 W/m²°C for acetone and 224.1 W/m²°C for graphene, as depicted in Fig. 6. Notably, graphene exhibits superior heat transfer coefficient readings when compared to acetone.

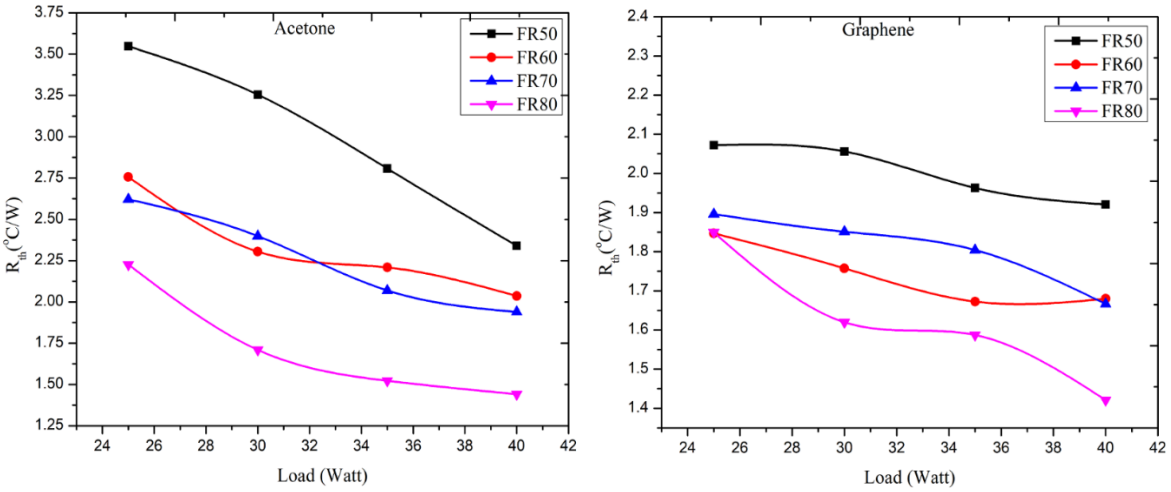

Figure 5. Effect of fill ratio on thermal resistance for acetone and graphene-based nano fluid.

  - Volume 18, Number 2 (ISSN 1995-6665)

5. Artificial Neural Network

Artificial Neural Networks (ANNs) utilizing Radial Basis Function (RBF) represent a machine learning model that amalgamates principles from both neural networks and radial basis functions. A radial basis function is a mathematical function that maps the distance between its input and a center point in a high-dimensional space. It is commonly used in interpolation and approximation tasks. In the context of ANNs, RBFs are used as activation functions within the hidden layers. A neural network that employs Radial Basis Function (RBF) typically consists of three layers: the input layer, hidden layer, and output layer. Each neuron in the input layer corresponds to a feature present in the input data (see Fig. 7 for reference). The hidden layer uses RBFs as activationfunctions. Each neuron in this layer is associated with a centre point in the input space. The RBF neurons compute the distance between the input data and their respective centers, then apply a radialbasis function to this distance to produce an activation value. The output layer produces the final predictions or classifications based on the activations from the hidden layer. RBF-based neural networks have certain advantages, such as good generalization capabilities and the ability to approximate complex functions. They can also handle noisy data to some extent. However, there arechallenges, such as determining the optimal number of RBF neurons and centres, which can impact model performance. RBF-based neural networks combine the radial basis function concept with neural network architecture to create a model that can effectively approximate functions and make predictions.

During the training process, the input parameters, as illustrated in Fig. 7, are fed into the neural network.

In Equation 3, as outlined in references [21, 22], the multiplication of input parameters (Mi) and a weight function (Wij) is totaled at the node junction, followed by the addition of the neuron's bias (bj). In this particular study, the input variables include the filler ratio, time duration, and heat input. Meanwhile, the output parameters being examined are temperature rise, heat transfer coefficient, and thermal resistance, as shown in Fig. 8.

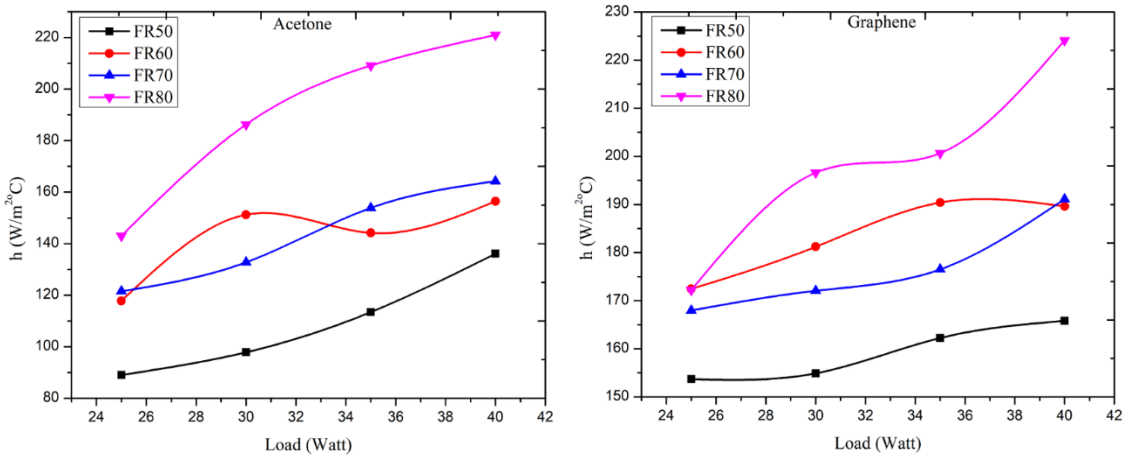

Figure 6. Effect of fill ratio on heat transfer coefficient for acetone and graphene based nano fluid

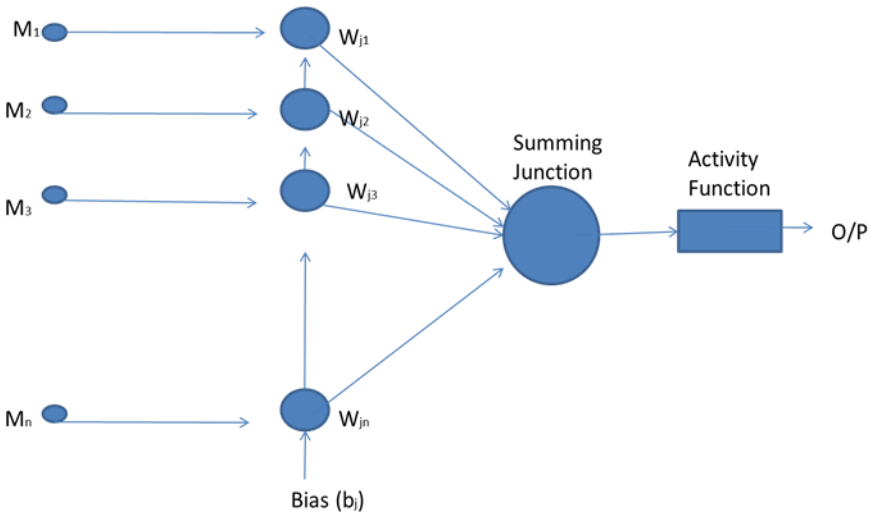

Figure 7. Generalized structure of artificial neurons

$$X = (\sum_{i=1}^{n} (W_{ij}M_i)) + b_j \quad (3)$$

The input data undergoes training through various learning algorithms, with Radial Basis Function (RBF) being a notably swifter choice compared to alternative algorithms [23]. The analysis involving artificial neural networks was carried out using Matlab software. The commonly employed activation function is the logsig function, which yields values within the range of -1 to +1 (as depicted in Equation 2), and it is expressed as:

$$X = 1/1+e^{-x} \quad (4)$$

The current research involves the utilization of three input variables to comprehensively analyze specific thermal properties. These variables encompass the temperature difference between the evaporator and condenser, the heat transfer coefficient, and the thermal resistance. The investigation process entailed the extraction of approximately 2000 distinct data sets from experimental trials. Thisextensive dataset was derived by systematically varying filler ratios (ranging from 50% to 80%), heatloads (ranging from 25W to 40W), and time intervals in seconds. This meticulous data collection approach allowed for a detailed assessment of the thermal characteristics exhibited by the studied nanofluids.

In the training process, input data is initially fed into the neural network and accumulated within the initial layer of nodes. The results from this first layer are then consolidated in the second layer, and this iterative process persists until the final output is generated from the neural network (refer to Fig. 8). Following this, the generated output is compared to the intended target output, and the resulting error is computed. To rectify this error, the weights within the network are adjusted in a backward propagation manner. However, it's worth noting a limitation of this weight adjustment equation: weights on a particular node cannot be identical to those on another node within the same layer because they would undergo identical adjustments during the training process. If all the weights within the neural network were initially set to zero, these weights would undergo identical adjustments across each layer. Mathematically speaking, this scenario would be equivalent to having just one node within each layer. This underscores the critical importance of initializing the weights in a multi-layer neural network with random values. Another rationale for this random initialization is to thoroughly explore the weight space, which does not behave like a quadratic function, unlike the linear perceptron. Utilizing randomly initialized weights adds complexity to accurately forecasting the initial performance of the control system.

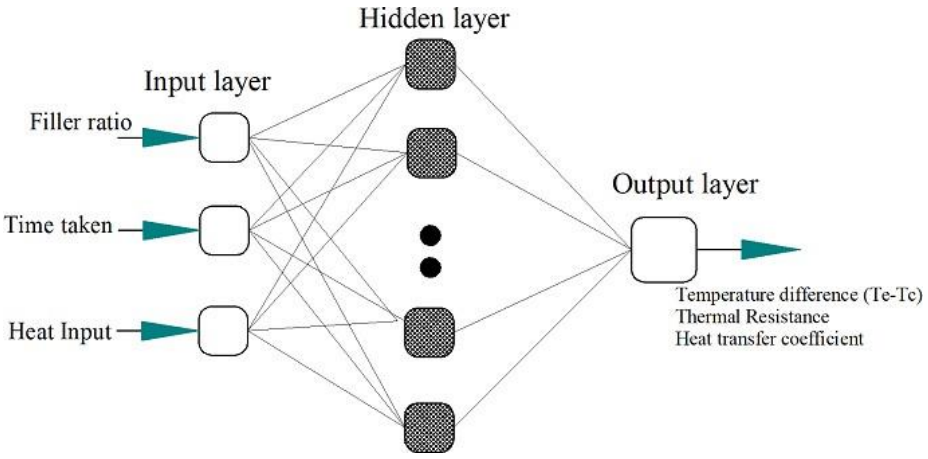

Figure 8. Developed neural network model for three different input parameters with three output.

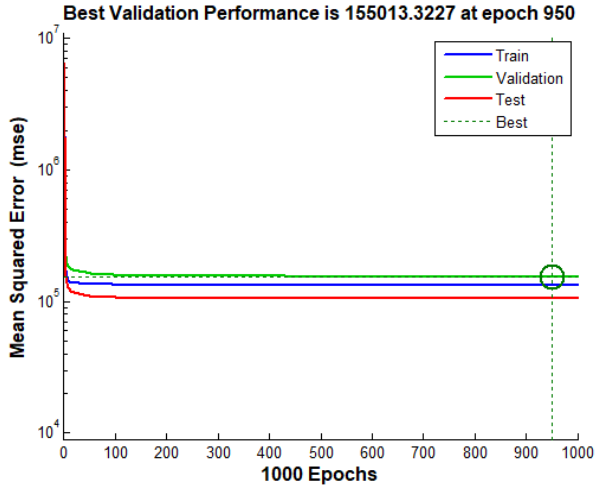

Figure 9. Mean square error for graphene nano fluid for 2000 data sets for acetone.

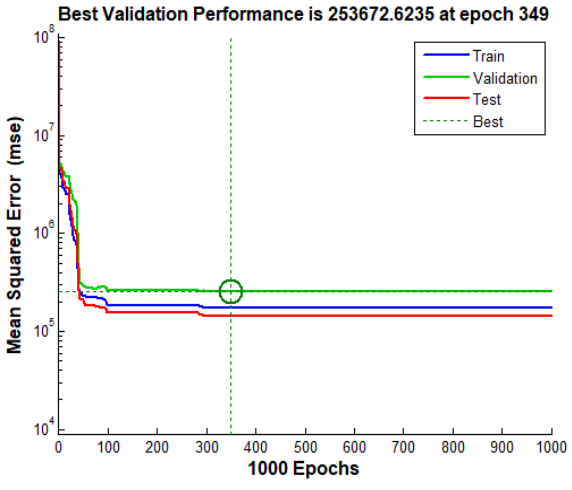

Figure 10. Mean square error for acetone nanofluidfor 2000 data sets for graphene.

Table 2. Weights and bias of the optimum model (3-4-3) for Graphene

Weights between the input and hidden layers (W4*3)
[67.0641 162.3513 -0.26999; -15.014 -13.8699 0.15233; -5.417 9.1206 -2.3186; 771.3941 -1551.1992 -3.4062]
Bias in hidden layer (B_{3*4})
[-511.0517 -442.1775 259.1736 121.3737; 8.6674 -264.5794 2.7325 9.5022; 1.9816 -183.7483 -271.1802 -209.6791]
Weights to output layer (W_{1*5})
[-122.6734; 2.3376; -3.9621; -2.3397]
Bias in output layer (B_{3*3})
[-27.182; 253.602; 213.23]

Table 3. Weights and bias of the optimum model (3-4-3) for acetone

Weights between the input and hidden layers (W_{4*3})
[-0.17966 -0.67108 -0.34595; -0.089199 -0.40247 -0.29606; -0.59899 1.6465 -0.12641; 0.4061 -3.2633 -10.4791]
Bias in hidden layer (B_{3*4})
[3.0488 -37.6016 19.7259 -0.22799; -14.3555 201.7166 -111.0656 -0.16134; -0.66344 -0.376 -1.5321 -0.53866]
Weights to output layer (W_{4*1})
[1.2418; 2.4402; 5.2771; 11.616]
Bias in output layer (B_{3*3})
[14.777; -76.7747; -1.8077]

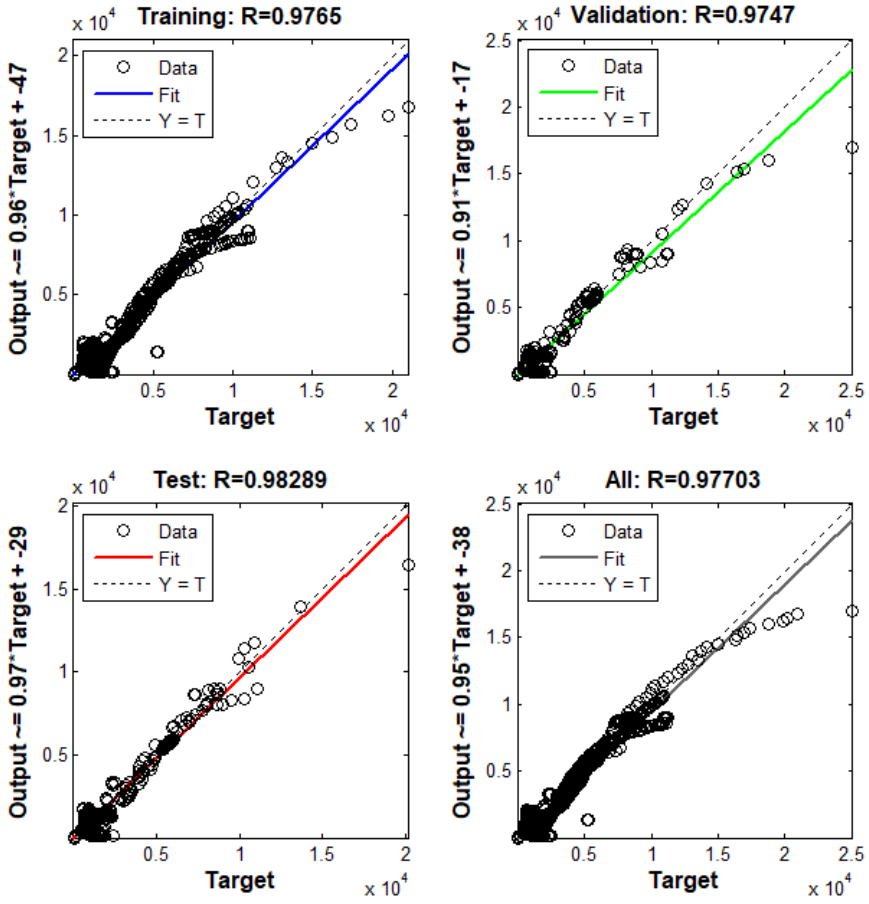

Figure 11. Regression analysis for training and testing for all combinations considered for graphene.

The effectiveness of the ANN in fitting experimental data is presented in a 3x3 matrix, which can be found in Tables 2 and 3. This matrix likely displays how well the ANN's predictions match the experimental data across different scenarios or parameters. The matrix shows the deviation between the magnitudes of the variables. This refers to the differences between the predicted values by the ANN and the actual experimental values. Most deviations are between zero to one, indicating that the ANN's predictions are generally close to the actual experimental values. A small portion of the data shows significant deviation, which means in some cases, the ANN's predictions were less accurate. A decrease in MSE with different neuron counts indicates that adjusting the number of neurons in the ANN can improve its accuracy. The correlation coefficients for acetone and graphene are presented in Figs 11 and 12, with the corresponding mean square error given in Table 4. The correlation coefficient measures the strength and direction of the linear relationship between the model's predictions and actual data for acetone and graphene.

The effectiveness of the Artificial Neural Network's (ANN) fit to the experimental data is depicted inthe 3 cross 3 matrix (Table, 2 and 3). It illustrates the deviation between the variable's magnitudes, wherein many clusters are around zero to one, and only a small fraction deviates

significantly from this central point. The decrease in Mean Squared Error (MSE) as neuron count varies highlightsone of the measurable outcomes, revealing the network's performance across different neuronquantities. The desired performance benchmark of 5×10^{-5} for the ANN has been successfully reached. A graphical representation of the network's performance is presented in Fig. 9 and 10 respectively. Finally, the coefficient correlation of acetone and graphene (Fig. 11 and 12) with mean square error is given in table 4.

To evaluate the deviation rate of the development model with the experimentation is based on these three performance parameters such as VAF, RMSE and MAPE. To assess the predictive capabilities of the models, performance predictions were defined using metrics such as VAF, RMSE, and MAPE. The respective equations for evaluating the predictive performance are presented in Equations 5, 6, and 7 [21]. RBNN Predicted R^2 values for acetone and graphene of these models during training, testing and validation is given in table 4.

$$\mathrm{VAF} = \left[1 - \frac{var(y-y')}{var(y)}\right] \times 100 \quad (5)$$

$$RMSE = \sqrt{\frac{1}{N}\sum_{i=1}^{N}(y - y')^2} \quad (6)$$

$$MAPE = \frac{1}{N}\sum_{i=1}^{N}\left|\frac{Ai-Pi}{Ai}\right| \times 100 \quad (7)$$

Comparison of the predicted data with experimental data of optimum RBFNN models with 3-5-3 for acetone and graphene was determined. Hence based on the observation the deviation between the measured value with RBFNN mode was less than 5% of the total number of data sets. Finally, RBFNN model shows the better performance to predict the temperature rise, heat transfer coefficient and thermal resistance in OHP with acetone and graphene respectively. The detail of probability lots for all the combinations of temperature differences, heat transfer rate and thermal resistance is shown in Figs 13 to 18 respectively.

Table 4. Overall regression for all the combinations considered for acetone and graphene

Random data			
Bayesian Regularization with radial basis function			
Coefficient of correlation (R)			
Total No. of data		Graphene	Acetone
Training	1700	0.9765	0.9718
Testing	300	0.9827	0.9731
Overall	2000	0.9770	0.9712
MSE	2000	1.0151	1.0641

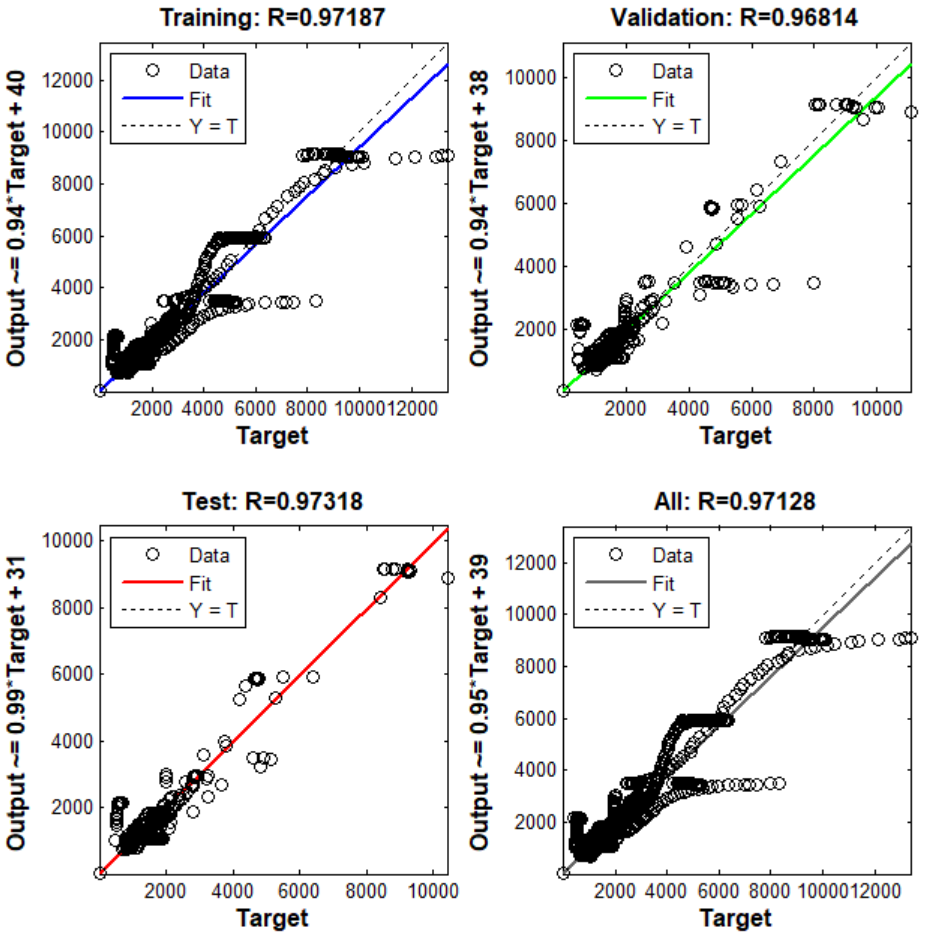

Figure 12. Regression analysis for training and testing for all combinations considered for acetone.

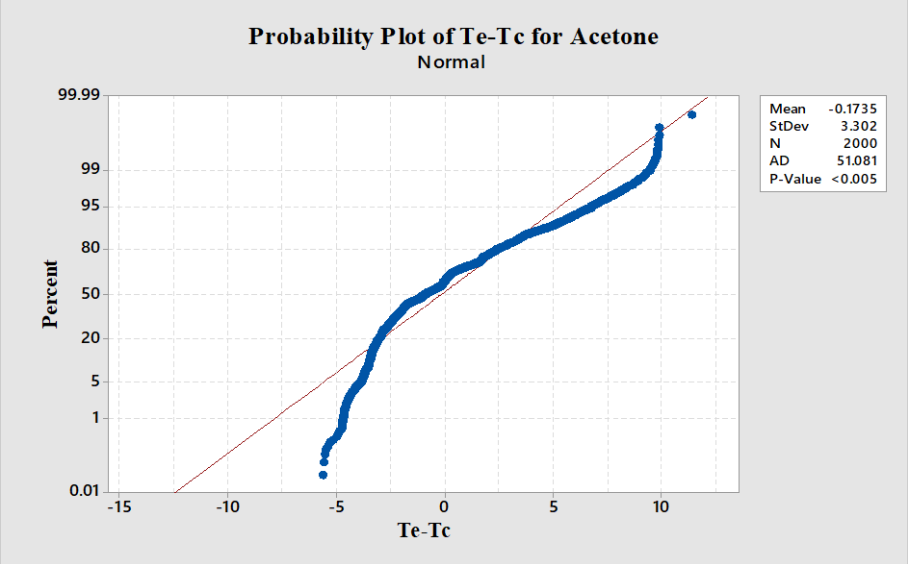

Figure 13. Probability plots of T_e-T_c for acetone.

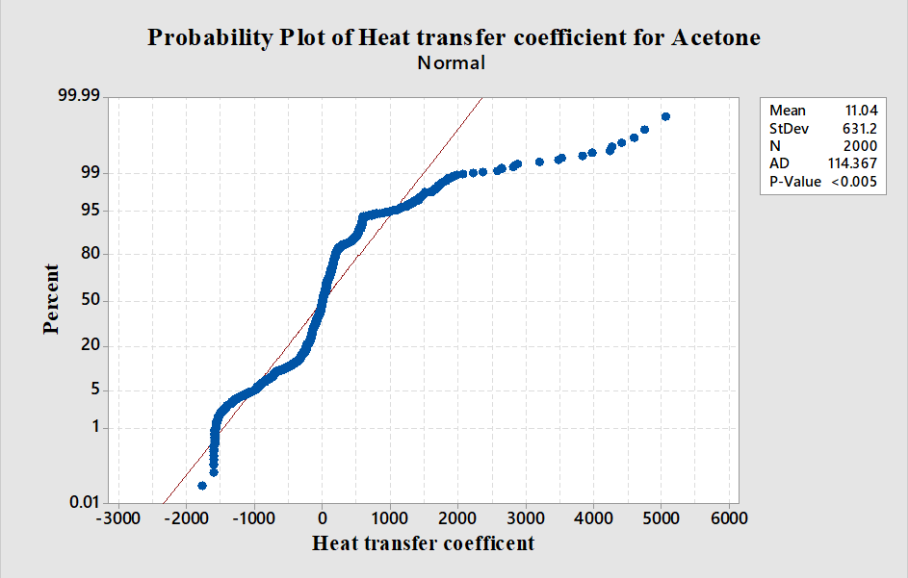

Figure 14. Probability plots of heat transfer coefficient for acetone.

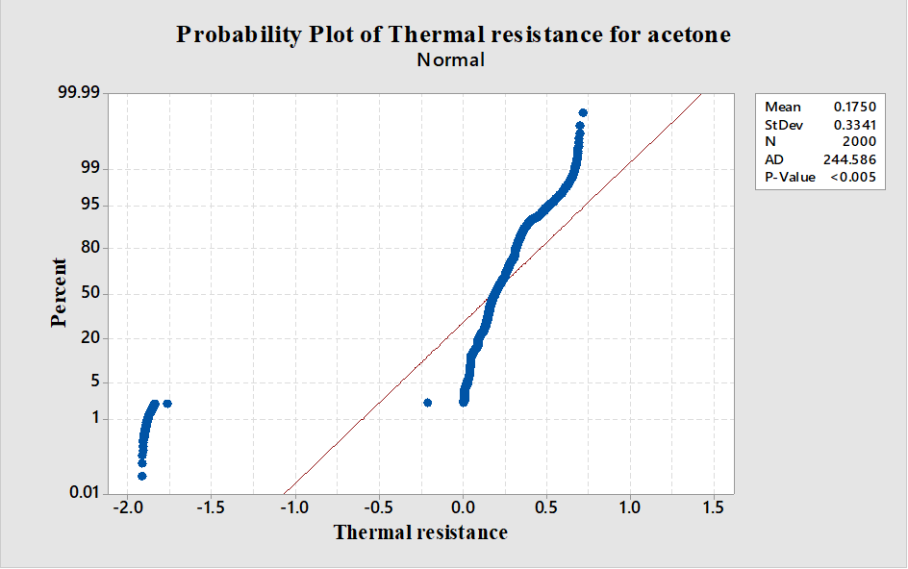

Figure 15. Probability plots of thermal resistance for acetone.

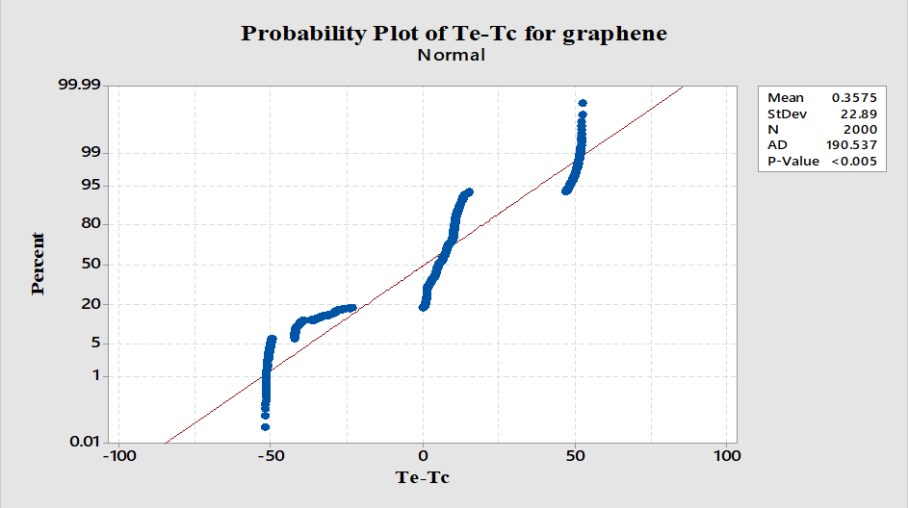

Figure 16. Probability plots of T_e-T_c for graphene.

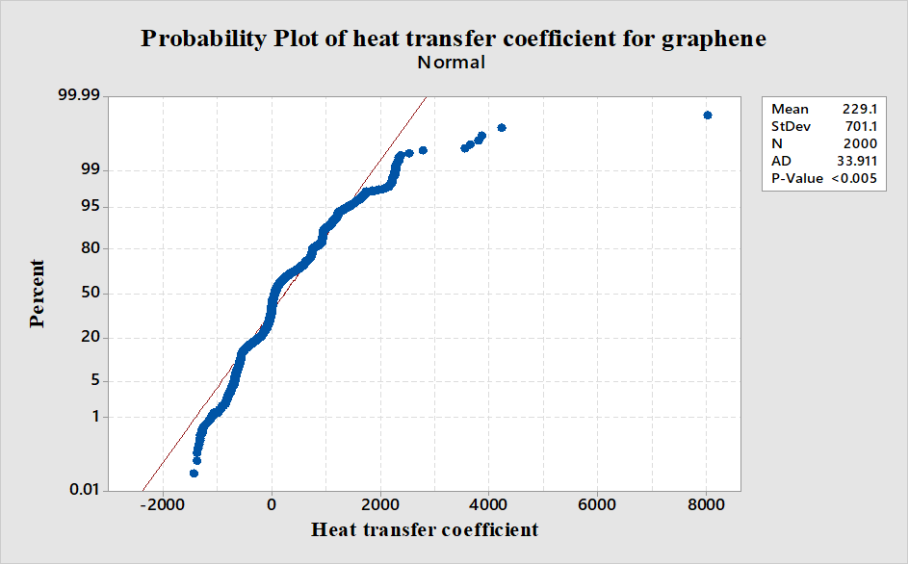

Figure 17. Probability plots of heat transfer coefficient for graphene

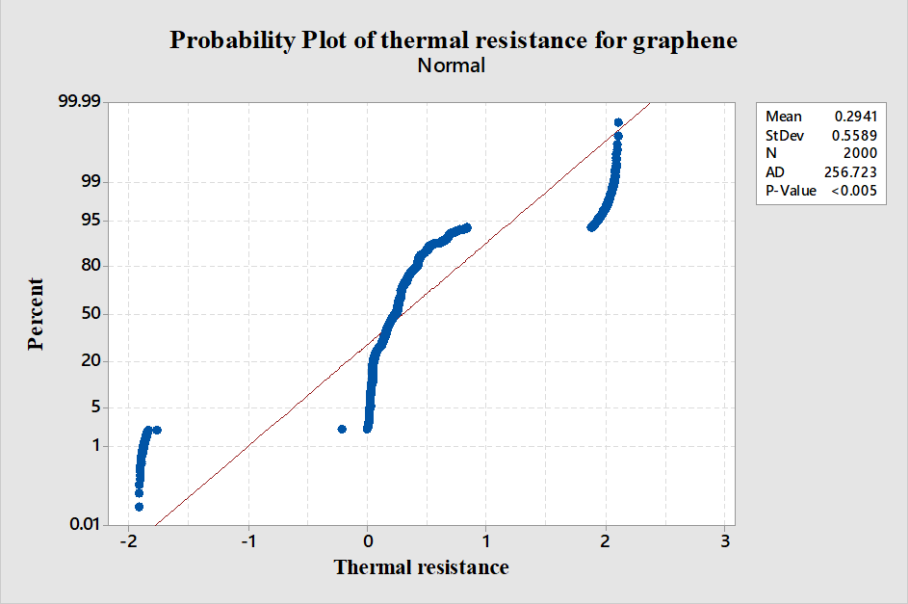

Figure 18. Probability plots of thermal resistance for graphene.

5.1. Error Analysis

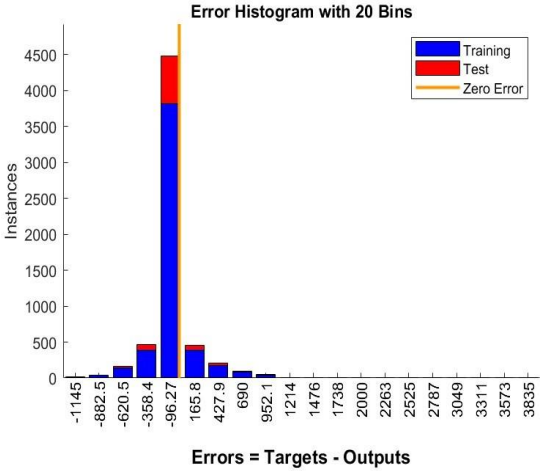

Figure 19. Error analysis based on input and outputvariables for graphene.

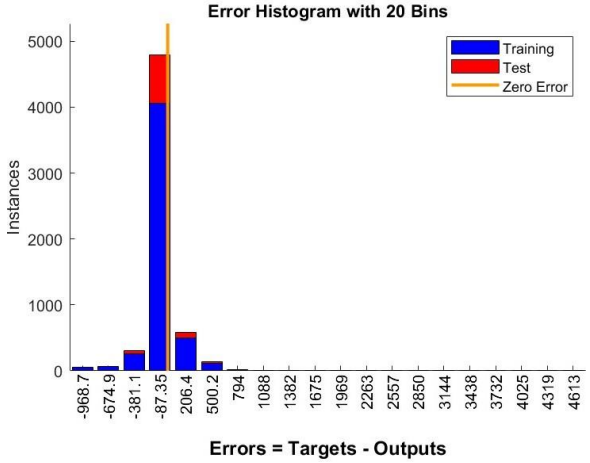

Figure 20. Error analysis based on input and outputvariables f or acetone.

Error analysis involves assessing the deviation or difference between the expected or desired output and the actual output obtained from a model, experiment, or simulation. It helps evaluate the accuracy and reliability of a model or experimental setup. In the present investigations zero error is shown at the testing and training section the Figs. 19 and 20 respectively. The maximum data for all the combinations considered is shown in the figure above. Overall, Figures 19 and 20 provide valuable information about the performance and reliability of models or experiments involving graphene and acetone, respectively, by evaluating the error associated with input and output variables.

6. Conclusions

In this study, an RBFNN (Radial Basis Function Neural Network) efficiently modeled temperature difference, heat transfer coefficient, and thermal resistance in graphene and acetone systems using three input parameters. Results indicate satisfactory modeling outcomes, and experimental datasets suggest that heat transfer coefficient increases with higher heat load across all combinations, while thermal resistance decreases with increased heat load.

- Acetone used as a base fluid in the present investigations due to its high volatility is perfect for heat pipes, when heated, it swiftly evaporates, boosting the heat transfer coefficient and effectively removing heat from the hot end. Additionally, acetone's boiling point can be adjusted by altering pressure, enabling its use in systems across various temperature ranges. This versatility makes acetone suitable for both low and high-temperature applications.
- The heat transfer coefficient for the graphene, operating at heat loads of 25W, 30W, 35W and40W, were recorded as 165.8,189.6, 191.1 and 224.1 W/m^2^{o}C, respectively. In contrast, the heat transfer coefficient for the acetone, under equivalent heat loads, yielded values of136.09, 156.44, 164.23 and 220.48 W/m^2^{o}C. Notably, the HTC for the acetone nanofluid exhibited a clear reduction when compared to the graphene.
- For graphene nanofluid at heat loads of 25W, 30W, 35W, and 40W, the recorded thermal resistances were 1.920, 1.679, 1.666, and 1.421 ºC/W, respectively. Meanwhile, acetone showed higher thermal resistances of 2.340, 2.035, 1.939, and 1.441 ºC/W under the same heat loads. This data highlights a significant reduction in thermal resistance for graphene compared to acetone.
- The 3-5-3 neural model successfully predicted key parameters such as temperature difference, heat transfer coefficient, and thermal resistance, with mean squared errors (MSE) of 1.015 for graphene and 1.064 for acetone. It also achieved high R-squared values (R2) of 0.977 for graphene and 0.973 for acetone. These results affirm that the RBFNN model's predictions are in close agreement with the experimental data, indicating its effectiveness in modeling the heat pipe's performance.

NOMENCLATURE

HTC- Heat Transfer coefficient (W/m^2^{o}C)
TR- Thermal resistance (^{0}C/W)
Q- Heat Input (W)
OHP –Oscillating heat pipe
ANN- Artificial Neural Network
MSE- Mean Squared Error
Te -Evaporator Wall Temperature (ºC)
Tc -Condenser Wall Temperature (ºC)
As-Surface area of OHP (m^2) t -Time (s)

References

[1] Yaxuan Xiong, Li Bo, Meng Qiang, Yuting Wu, Xingxing Zhang, Peng Xu,Chongfang M, “A characteristic study on the start-up performance of molten-salt heatpipes: Experimental investigation”, Experimental Thermal and Fluid Science, Vol. 82, 2017, pp. 433–438.

[2] Hua Han, Xiaoyu Cui, Yue Zhu, Shende Sun, “A comparative study of the behavior of working fluids and their properties on the performance of pulsating heat pipes (PHP)”, International Journal of Thermal Sciences, Vol. 82, 2014, pp. 138-147.

[3] S.M. Sohel Murshed, C.A. Nieto de Castro, “A critical review of traditional and emerging techniques and fluids for

electronics cooling", Renewable and Sustainable Energy Reviews, Vol. 78, 2017, pp. 821–833.

[4] Ziang Chena, Xinghua Tonga , Hai Liua , Chunsheng Guoa, Fangyi Qua , Huisheng Cong, "A design of the Micro-Plate Loop Heat Pipe and development of the porous nickel capillary wick", Procedia Engineering, Vol. 205, 2017, pp. 3931–3937.

[5] Reza Nemati, Mohammad Behshad Shafii, "Advanced heat transfer analysis of a U- shaped pulsating heat pipe considering evaporative liquid film trailing from its liquid slug", Applied Thermal Engineering, Vol. 138, 2018, pp. 475–489.

[6] M. Mameli, D. Mangini, G.F.T. Vanoli, L. Araneo, S. Filippeschi, M. Marengo, "Advanced multi-evaporator loop thermosyphon", Energy 112, 2016, 562-573.

[7] Soo-Jin Jeong, "A full transient three-dimensional study on the effect of pulsating exhaustflow under real running condition on the thermal and chemical behavior of closed-coupled catalyst", Chemical Engineering Science, Vol. 117, 2014, pp. 18–30.

[8] Stéphane Lips, Frédéric Lefèvre, " A general analytical model for the design of conventional heat pipes", International Journal of Heat and Mass Transfer, Vol. 72, 2014, pp. 288–298.

[9] Tomasz Pałczyński, "A hybrid method of estimating pulsating flow parameters in the space-time domain", Mechanical Systems and Signal Processing, Vol. 89, 2017, pp. 58–66.

[10] G. Gürsel, A.J.H. Frijns, F.G.A. Homburg, A.A. van Steenhoven, "A mass-spring- damper model of a pulsating heat pipe with a non-uniform and asymmetric filling", Applied Thermal Engineering, Vol. 91, 2015, pp. 80-90.

[11] How Ming Lee, Heng Yi Li, "A mathematical model for estimation of the maximum heattransfer capacity of tubular heat pipes", Energy Procedia, Vol. 142, 2017, pp. 3908–3913.

[12] Mobin Arab, Ali Abbas, (2014), "A model-based approach for analysis of working fluids in heat pipes", Applied Thermal Engineering, Vol. 73, 2014, pp 751-763.

[13] J. Gabriel Monroe, Zachary S. Aspin, John D. Fairley, Scott M. Thompson, "Analysis and comparison of internal and external temperature measurements of a tubular oscillating heat pipe", Experimental Thermal and Fluid Science, Vol. 84, 2017, pp. 165–178.

[14] Vivek K. Patel, "An efficient optimization and comparative analysis of ammonia and methanol heat pipe for satellite application", Energy Conversion and Management, Vol. 165, 2018, pp. 382–395.

[15] Yulong Ji, Gongwei Liu, Hongbin M, Gen Li, Yuqing Sun, "An experimentalinvestigation of heat transfer performance in a polydimethylsiloxane (PDMS) oscillating heat pipe" Applied Thermal Engineering, Vol. 61, 2013, pp. 690-697.

[16] Durga Bastakoti, Hongna Zhang, Weihua Cai, Fengchen Li, "An experimental investigation of thermal performance of pulsating heat pipe with alcohols and surfactant solutions", International Journal of Heat and Mass Transfer, Vol. 117, 2018, pp. 1032–1040.

[17] M Lutfor Rahman, Rasel A Sultan, T Islam, Noor M Hasan, Mohammad Ali, "An experimental investigation on the effect of fin in the performance of closed loop pulsating heat pipe (CLPHP)", Procedia Engineering, Vol. 105, 2015, pp. 137 – 144.

[18] Omar T. Ibrahim, J. Gabriel Monroe, Scott M. Thompson, Nima Shamsaei, HassinaBilheux, Alaa Elwany, Linkan Bian, "An investigation of a multi-layered oscillating heat pipe additively manufactured from Ti-6Al-4V powder", International Journal of Heat and Mass Transfer,Vol. 108, 2017, pp. 1036–1047.

[19] Chih-Yung Tseng, Kai-Shing Yang, Kuo-Hsiang Chien, Shih-Kuo Wu, Chi-Chuan Wang, "A novel double pipe pulsating heat pipe design to tackle inverted heat source arrangement", Applied Thermal Engineering Vol. 106, 2016, pp. 697–701.

[20] Durga Bastakotia, Hongna Zhanga, Da Lia , Weihua Caia, Fengchen Lib, "An overview on the developing trend of pulsating heat pipe and its performance", Applied Thermal Engineering Vol. 141, 2018, pp. 305–332.

[21] Vijay Kumar S, B. M. Kunar, Ch. S. N. Murthy, "ANN model for prediction of bit-rock interface temperature during rotary drilling of limestone using embedded thermocouple technique", Journal of Thermal Analysis and Calorimetry, Vol. 139, No. 3, 2020, pp. 2273-2282.

[22] Vijay Kumar S, B. M. Kunar, Ch. S. N. Murthy, M. R. Ramesh, "Measurement of bit-rockinterface temperature and wear rate of the tungsten carbide drill bit during rotary drilling", Friction, Vol. 8, No. 6, 2020, pp. 1073-1082.

[23] Vijay Kumar S, B. M. Kunar, Ch. S. N. Murthy, "Experimental investigation and statistical analysis of operational parameters on temperature rise in rock drilling", International Journal of Heat and Technology, Vol. 36, No. 4, 2018, pp. 1174-1180.

[24] Xinjun Su, Ming Zhang, Wei Han, Xianmin Guo, "Experimental study on the heat transfer performance of an oscillating heat pipe with self-rewetting nanofluid", International Journal of Heat and Mass Transfer, Vol. 100, 2016, pp. 378–385.

[25] Yu Zhou, Xiaoyu Cui, Jianhua Weng, Saiyan Shi, Hua Han, Chengmeng Chen, "Experimental investigation of the heat transfer performance of an oscillating heat pipe with graphene nanofluids", Powder Technology, Vol. 332, 2018, pp. 371–380.

[26] R. Naik, V. Varadarajan, G. Pundarika and K. R. Narasimha, "Experimental Investigation and Performance Evaluation of a Closed Loop Pulsating Heat Pipe", Journal of Applied Fluid Mechanics, Vol. 6, No. 2, 2013, pp. 267-275.

[27] P. Venkataramana, P. Vijayakumar and B. Balakrishna, "Experimental Investigation of Aluminum Oxide Nanofluid on Closed Loop Pulsating Heat Pipe Performance", Journal of Applied Fluid Mechanics, Vol. 15, No. 6, 2022, pp. 1947-1955.

[28] Abdollahi, A. Rafiei, M. Ahmadi, M. Pourjafar-Chelikdani, and K. Sadeghy, "Dynamics of Microbubbles Oscillating in Rheopectic Fluids Subject to Acoustic Pressure Field", Journal of Applied Fluid Mechanics, Vol. 16, No. 10, 2023, pp. 1916-1926.

[29] Rafik Bouakkaza, Yacine Khelilia, Faouzi Salhib, "Unconfined Laminar Nanofluid Flow and Heat Transfer Around a Square Cylinder with an Angle of Incidence", Jordan Journal of Mechanical and Industrial Engineering, Vol. 13 No. 3, 2019, 191-196.

[30] Rashid Ali, Anshumaan Singh, "Numerical Study of Fluid Dynamics and Heat Transfer Characteristics for the Flow Past a Heated Square Cylinder", Jordan Journal of Mechanical and Industrial Engineering, Vol. 15, No. 4, 2021, pp. 357-376.

[31] Ittedi Shravani, Dodda Ramya, Sucharitha Joga, "MHD Tangent Hyperbolic Nanofluid with Zero Normal Flux of Nanoparticles at the Stretching Surface with Thermal Radiation", Jordan Journal of Mechanical and Industrial Engineering, Vol. 12, No. 3, 2018, pp. 171-177.

[32] Iman Zahmatkesh, Seyyed Ali Naghedifar, "Pulsating Nanofluid Jet Impingement onto a Partially Heated Surface Immersed in a Porous Layer", Jordan Journal of Mechanical and Industrial Engineering, Vol. 12, No. 2, 2018, pp. 99-107.

[33] T. Vijaya Laxmi, Bandari Shankar, "Radiative Boundary Layer Flow and Heat Transfer of Nanofluid over a Nonlinear Stretching Sheet with Slip Conditions and Suction", Jordan Journal of Mechanical and Industrial Engineering, Vol. 10, No. 4, 2016, pp. 285-297.

[34] Mohammad Saraireh, "Computational Fluid Dynamics Simulation of Plate Fin and Circular Pin Fin Heat Sinks",

Jordan Journal of Mechanical and Industrial Engineering, Vol. 10, No. 2, 2016, pp. 99-104.

[35] Louy Qoaider, Suhil Kiwan, Qahtan Thabit, "Investigation of the Flowability and the Thermal Behavior of Sand /Basalt-Mixture in Moving Bed Heat Exchanger (MBHX) as Heat Transfer Medium for Concentrating Solar Tower Plants", Jordan Journal of Mechanical and Industrial Engineering, Vol. 10, No. 4, 2016, pp. 263-270.

[36] T. Vijaya Laxmi, Bandari Shankar, "Radiative Boundary Layer Flow and Heat Transfer of Nanofluid over a Nonlinear Stretching Sheet with Slip Conditions and Suction", Jordan Journal of Mechanical and Industrial Engineering, Vol. 10, No. 4, 2016, pp. 285-297.

[37] Ahmad K AL-Migdady, Ali M Jawarneh, Hussein N Dalgamoni, Mohammad Tarwaneh, "Combined Effects of Eccentricity and Internal Fins on the Shell and Tube Latent Heat Storage Systems", International Journal of Recent Technology and Engineering (IJRTE), Vol. 9, No. 1, 2020, pp. 230-236.

[38] Ali M. Jawarneh, Mohamad Al–Widyan, Zain Al-Mashhadani, "Experimental Study on Heat Transfer Augmentation in a Double Pipe Heat Exchanger Utilizing Jet Vortex Flow", Heat Transfer, Vol. 52, No. 1, 2023, pp. 317-332.